PAPER

Check for updates

Advancing sustainability: a novel biopolymer-based degradable nanoclay composite film for next-generation packaging†

Zeba Tabassum,[a] Madhuri Girdhar,*[b] Tabarak Malik, ID *[c] Anil Kumar[d] and Anand Mohan[a]

Global concerns are increasing worldwide owing to the utilization of non-renewable fossil fuel-derived polymeric films for the packaging of perishables and other related commodities. The emergence of bio-based packaging films, characterized by affordability, environmental friendliness, and abundant renewable sources, offers a promising alternative to address these concerns. This study aims to mitigate the adverse impacts associated with petroleum-based films by developing an effective bio-nanocomposite with enhanced mechanical and barrier properties. The developed composite, achieved through the incorporation of montmorillonite (MMT) nanoclay into two distinct biopolymer blends (chitosan–xanthan gum and chitosan–vanillin), was further optimized to determine the optimal ratio. The bio-nanocomposite film with 3% nanoclay reinforcement in the chitosan–vanillin blend demonstrated superior performance compared to all other films. In contrast to an untreated chitosan film, this bio-nanocomposite exhibited reduced transmittance, mitigating oxidative damage from UV radiation in packaged food items. Notably, a substantial improvement in water resistance and a remarkable 6.64-fold increase in tensile strength were observed. The film's biodegradability, as evidenced by a 25% weight loss in the first month in a soil burial test, underscores its environmental friendliness. Results from a range of instrumental techniques and measurements collectively suggest that the synthesized and optimized film has significant potential for application in the future sustainable food-packaging industry.

1. Introduction

Food safety and preservation are the top priorities in food businesses and enterprises. Food packaging safeguards perishables from outside influences that can affect their quality, safety, and shelf life.[1] Commercially popular plastic packaging materials, including low-density and high-density polyethylene, polycarbonate, polyethylene terephthalate, polyvinyl chloride, polypropylene, polystyrene, and polyamides, have been widely adopted in the food industry because of their cost-effectiveness, lightweight nature, and robust performances. However, the pervasive use of non-biodegradable plastic packaging has

resulted in a concerning surge in environmental challenges; for instance, over 8 million metric tons of plastic waste are dumped into the oceans annually as a result of the widespread use of petroleum-based plastics and the dearth of suitable disposal solutions. By 2025, it is anticipated that between 100 and 250 million metric tons of improperly disposed plastic waste—the majority of which comes from coastal areas—will be in the ocean. Due to their innate eco-friendliness, natural fiber-reinforced composites have become increasingly popular and have a lower carbon footprint.[2,3] Some examples of biodegradable polymers include cellulose, starch, chitosan, collagen, gelatin, and xanthan gum.[4] Chitosan, one of the many biopolymers, has a reputation for being a flexible option due to its capacity for superior film formation, lack of toxicity, widespread accessibility, and great biodegradability. It has undergone substantial research for applications such as bone tissue engineering, water purification, medication delivery, cosmetics, and food packaging.[4] According to research, adding additional substances can be a wonderful way to enhance its inherent drawbacks, such as poor mechanical or barrier qualities. The bacteria xanthomonas campestris secretes a high molecular weight extracellular polysaccharide known as xanthan gum.

[a] School of Bioengineering and Biosciences, Lovely Professional University, Phagwara, Punjab, 144401, India

[b] Division of Research and Development, Lovely Professional University, Phagwara, Punjab, 144401, India. E-mail: madhurigirdhar007@gmail.com

[c] Department of Biomedical Sciences, Institute of Health, Jimma University, Ethiopia. E-mail: tabarak.malik@ju.edu.et

[d] Gene Regulation Laboratory, National Institute of Immunology, New Delhi 110067, India

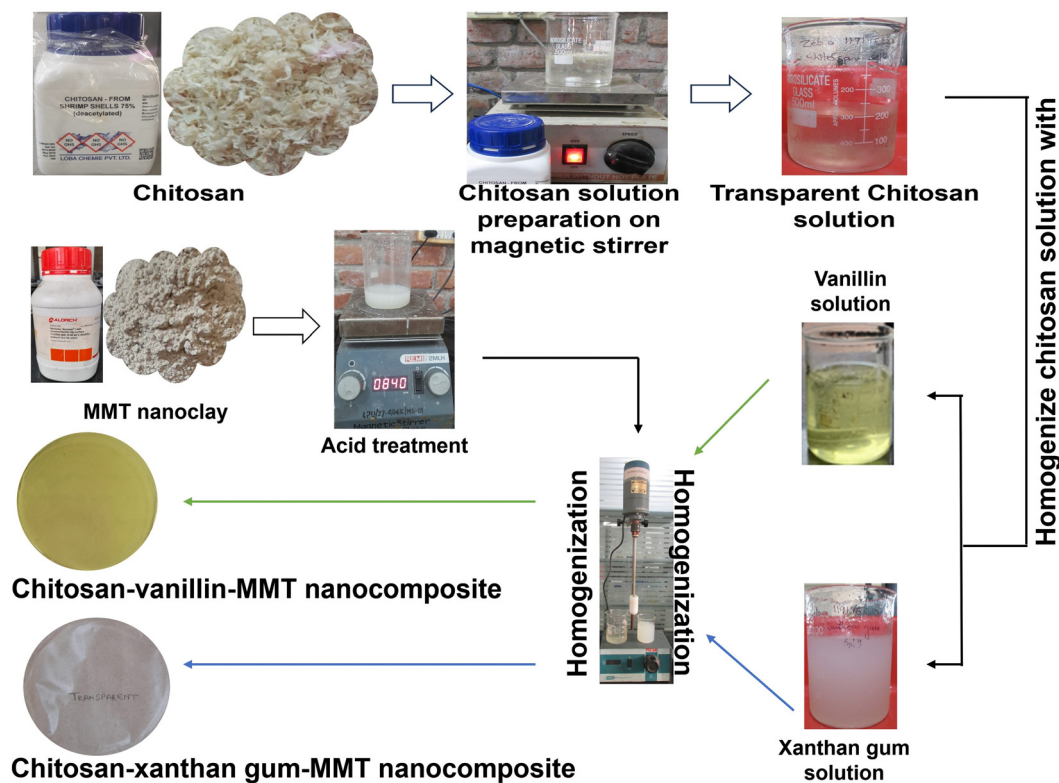† Electronic supplementary information (ESI) available. See DOI: **https://doi.org/10.1039/d4ma00476k**

Fig. 1 Film preparation.

The long-chain polymer xanthan gum, with its functional groups, enhances the mechanical attributes of biodegradable materials by improving their film-forming capabilities, tensile strength, and elasticity when combined with other biopolymers or nanomaterials.[5] Vanillin is the primary component of the extract of vanilla bean, and is typically used as a flavoring agent and is also able to improve various characteristics of films, including their tensile strength, and stability, while also decreasing their water vapor and oxygen permeability.[6,7] Montmorillonite nanoclay is one of the nanofillers that is a popular choice among scientists. The more twisted paths and compact structures that are produced through the interactions with the polymeric chains increase its barrier properties against moisture and gases. Also, due to its low cost, high abundance, mechanical resistance, swelling and plasticizer abilities, montmorillonite (MMT), a layered silicate mineral clay, is the most studied and used nanomaterial for this purpose.[8–10]

Therefore, the primary objectives of the present research were to fabricate two different types of chitosan-based composites, namely chitosan–xanthan gum and chitosan–vanillin blend films, followed by their incorporation with montmorillonite nanoclay to investigate high performance chitosan-based blend films. Moreover, their structural changes and functional properties of the films were also explored through a variety of instrumental techniques and multiple laboratory scale tests. An optimization study was carried out to find out the best composite film for its potential use in biodegradable food-packaging

applications, which has not been previously studied or reported before.

2. Experimental section

2.1 Materials

Chitosan from shrimp shells (75% deacetylated), xanthan gum pure (Food Grade), glacial acetic acid (99.5% extra pure), glycerol (purified), vanillin, anhydrous $CaCl_2$, and NaCl were procured from Loba Chemie Pvt. Ltd, India. Ethanol was bought from LABOGENS China. Montmorillonite nanoclay (surface modified with 35–45 wt% dimethyl dialkyl amine) was purchased from Sigma Aldrich.

2.2 Methodology

2.2.1 Fabrication of packaging films. The packaging materials were fabricated through a solution casting technique at room temperature following the methodology outlined previously by several researchers,[8,9,11–15] albeit with slight modifications. Chitosan was utilized as the primary matrix, and blended with xanthan gum and vanillin separately, in different ratios, followed by the incorporation of montmorillonite nanoclay in different wt%. Fig. 1 displays the film-fabrication strategy.

A pure form of chitosan packaging film was synthesized following the method outlined in previous research.[12,16] To

Table 1 Components used and their respective composition to prepare films for the further tests

S. no.	Chitosan	Xanthan gum	Vanillin	Montmorillonite nanoclay (%)	Remarks	Selection	Film code
1	1%	NA	NA	NA	Good film	Selected as the control	C
2	1%	NA	0.5	NA	No strength improvement	NA, Rejected	NA
3	1%	NA	1	NA	Good film	Selected for nanocomposite preparation	NA
4	1%	NA	1.5	NA	Stiffness	NA, rejected	NA
5	1%	0.5	NA	NA	Good film	Selected for nanocomposite preparation	NA
6	1%	1	NA	NA	Lack transparency	NA, rejected	NA
7	1%	1.5	NA	NA	Brittle film	NA, rejected	NA
8	1%	0.5	NA	1	Good film	Selected; for further testing	CXM1
9	1%	0.5	NA	3	Good film	Selected; for further testing	CXM3
10	1%	0.5	NA	5	Good film	Selected; for further testing	CXM5
11	1%	0.5	NA	7	Brittleness	NA, rejected	NA
12	1%	NA	1	1	Good film	Selected; for further testing	CVM1
13	1%	NA	1	3	Good film	Selected; for further testing	CVM3
14	1%	NA	1	5	Stiff and opaque	NA, rejected	NA

manufacture the pristine chitosan film (1%), chitosan flakes were dissolved in a water-based solution containing 1% glacial acetic acid. The solution was left at room temperature on a magnetic stirrer for 1 h to ensure complete dissolution and the formation of a clear solution. Later, 20 ml samples of this solution were cast on separate Petri dishes of 9.5 cm diameter and kept for drying.[12,16] By gradually dissolving the powdered form of xanthan gum in distilled water, under constantly rotation with a magnetic stirrer using a magnetic bead at ambient room temperature (25–27 °C) for 30 min, xanthan gum solutions were obtained. Blends of biopolymers, *i.e.*, chitosan and xanthan gum, were fabricated using the approach outlined by other researchers previously.[17] The chitosan and xanthan gum blends were crafted through homogenization for 10 min. Subsequently, the ultimate homogenized solution was then cast onto a Petri plate and allowed to air dry at ambient temperature (25–27 °C).[16,17] Vanillin solution was prepared by dissolving vanillin powder in ethanol, with continuous agitation using a magnetic stirrer until complete dissolution was achieved. Simultaneously, a chitosan solution was prepared using a similar method previously mentioned. Thereafter, the two solutions were homogenized through continuous stirring using a magnetic stirrer to produce a blended solution.[7,18] To fabricate the nanocomposites (chitosan–xanthan gum–montmorillonite and chitosan–vanillin–montmorillonite), montmorillonite nanoclay was acid (1% glacial acetic acid) treated overnight and slowly added to both types of blended solution, and kept on a magnetic stirrer for another 4 h for proper mixing. The resultant solution was poured in a Petri dish and kept to air dry at room temperature for the next 2 days. All the resultant thin film was peeled off carefully after drying and kept in a desiccator until further use.[8,15]

As shown in Table 1, 6 types of packaging films were finally chosen for further evaluation. For each type of tested specimen, experimentation was done in triplicate. For the characterization tests by FE-SEM, TGA, FTIR, and mechanical testing, film samples of 1 cm^2 were used, while for the UV-vis spectroscopy analysis, film samples of 3 cm^2 were used.

2.2.2 Analytical characterization. To reveal important insights regarding the structural morphology of the created

films, they were thoroughly analyzed by different characterization techniques as follows.

To investigate the interactions of the materials through the bond formation and the presence of functional groups in the manufactured films, Fourier transform infrared spectroscopy (FTIR) was implemented, using a Fourier transform infrared spectrometer from PerkinElmer, with spectrum 10 software. Here, 0.5 cm^{-1} resolution was utilized for generation of the FTIR spectra in the transmission mode in the 400–4000 cm^{-1} range.[8,16,19,20]

A universal testing machine (Zwick Roell, Germany Static UTM Z010) was used to evaluate the mechanical attributes in terms of the tensile strength (MPa) and elongation at break (%) of the films at room temperature and at a cross-head speed of 10 mm min^{-1}.[16,21–24]

Thermogravimetric analysis (TGA) and its corresponding curves were used to assess the thermal stability of the materials, which was carried out using a thermogravimetric analyzer (PerkinElmer) in a nitrogen environment at a heating rate of 10 °C min^{-1} in the temperature range of 30 °C to 500 °C.[8,16,22,24]

To analyze the surface appearance and the thickness of the films, field emission scanning electron microscopy (FE-SEM) was utilized with a JEOL instrument. The microscopic imaging process involved yielding visuals at various magnifications and employing accelerated voltages set at 5 and 10 kV. For the measurements of the thickness of all the thin films, SEM micrographs were obtained at various parts, and the average thickness was estimated. A conductive layer of gold was applied on all the film samples to mitigate surface charging.[16,23,25,26]

The opacity of the synthesized films was calculated with the equation: opacity = Abs$_{600}$/thickness (mm), with the absorbance recorded using a LI-2800 UV-vis double beam spectrometer. In the analysis, the film samples were cut into rectangular shapes and placed inside a quartz cuvette to measure the absorbance at 600 nm.[16,25–28]

2.2.3 Barrier property. The water vapor transmission rate (WVTR) of the created packaging films was calculated following a procedure outlined by previous scholars.[16,29,30] Here, the films under examination were securely affixed to the aperture

of a glass vial containing pre-measured anhydrous calcium chloride (CaCl$_2$). Subsequently, these vials were positioned within a desiccator containing a saturated sodium chloride (NaC) solution, ensuring a consistent relative humidity of 75 ± 5%. The WVTR of the films, expressed in g m^{-2} day^{-1}, was determined using the formula WVTR = W/S, wherein the weight gain of the glass vial (W) and the surface area of the film exposed to the experimental conditions (S) were measured before and after a single day of testing.

The evaluation of the film's gas barrier characteristics also included an oxygen transmission test. Analysis of the oxygen permeability followed a methodology described in previous research, including our own prior research contributions.[16,27,28,30,31] Subsequently, the films were enveloped around the aperture of glass vials and hermetically sealed with a strip. These sealed vials were then housed in a desiccator at ambient temperature (25–27 °C). Over a three-day period, the mass of each vial was meticulously measured once per day. The subsequent equation was employed to compute the oxygen permeability transmission rate (OPTR): OPTR = slope/film area.

To ascertain the UV-light-obstruction characteristics, the absorbance of the films was assessed employing a UV-visible spectrophotometer within the wavelength range of 280–800 nm. For the spectrophotometric analysis, the test films were segmented into rectangular sections measuring 3 × 1 cm^2 and positioned within a quartz cuvette. A counterpart cuvette was maintained empty for control purposes.[16,27,28,32]

2.2.4 Water absorbency and degradability. All of the films' ability to absorb water was examined in terms of the percentage swelling ratio, which was tested by cutting each film sample into a small square, weighing it (initial weight W_1), and then submerging it totally in deionized water for one day to allow for adequate water absorption. After the films had sufficiently swelled, they were removed from water, with any extra water was scraped off the surface using filter paper, and the final weight (W_2) was recorded. Using the following formula, the films' capacity to absorb water was determined. Swelling ratio (%) = $W_2 - W_1/W_1 \times 100$, where W_1 and W_2 are the weights of the dry and swollen samples, respectively.[16,25,27,33]

In order to evaluate the biodegradability of the biopolymer-based films, a biodegradation assessment was conducted by interring the films in soil and monitoring their weight loss. Daily, the soil received a sprinkling of tap water to sustain moisture, with excess water draining away through a bottom pot drainage hole. Prior to burial in freshly excavated field soil within a pot, all the films underwent pre-weighing (W_i). At seven-day intervals, the biodegradation of the film samples was measured by delicately extracting them from the soil, rinsing in distilled water to eliminate soil residues, desiccating, and then reweighing (W_f). Furthermore, the weight or degradation% = $W_i - W_f/W_i \times 100$.[16,28,34,35] Physiochemical analysis (pH and N, P, K) of the soil utilized in the biodegradation experiments was done by submitting the soil samples to IRCLASS Systems & Solutions Pvt. Ltd for analysis using standard methods.

3. Result and discussion

3.1 Analytical characterization

The solution casting method was employed exclusively for the synthesis of the chitosan-based nanocomposite films, chosen for its cost-effectiveness and ease of preparation. Here, prolonged drying periods at lower temperatures induces the reorganization of the solution structure, enhancing the interaction of the hydrophilic tails of chitosan with water molecules through hydrogen bonds and van der Waals forces.[16,36] Two distinct blends, incorporating xanthan gum and vanillin, were meticulously crafted utilizing chitosan as the primary matrix, followed by reinforcement with surface-modified montmorillonite nanoclay in various ratios. Notably, in the xanthan gum blends, an optimal ratio of 0.5% xanthan gum proved efficacious, as surpassing this proportion led to film brittleness. Conversely, in the vanillin blends, exceeding a 1 : 1 ratio resulted in alterations in the color parameters and opacity of the film. These formulations underwent the intricate process of nanocomposite formation. In the case of the chitosan–xanthan gum–nanoclay films, exceeding 5 wt% nanofillers, and in the case of chitosan–vanillin–nanoclay films, surpassing 3 wt% nanofillers, led to a compromise in their flexibility and transparency, as depicted in Table 1. Among all the formulations tried and tested, six were meticulously chosen for further comprehensive investigations, as illustrated in Fig. 2. A noteworthy phenomenon observed in all the films was the glossier appearance of the bottom side compared to the upper side. This peculiarity was attributed to the evaporation of moisture from the topmost part of the film in the casting tray, an aspect noted by other researchers[37] and corroborated by our earlier published study.[16]

3.1.1 Thickness measurement. The thickness of bio-based packaging materials is pivotal in determining their physical properties, including their strength, and optical and barrier properties, all of which are vital factors in ensuring the protection and preservation of food products. The thickness of the films remained relatively unchanged, regardless of whether the pristine biopolymer (C) or biopolymer-based nanocomposites (CXM1, CXM3, CXM5, CVM1, CVM3) with different ratios. However, there was a slight increase observed, going from 0.05 mm in the control group (C) to 0.1 mm in the group with a specific nanocomposite ratio (CXZ5). The exact measurements are detailed in Table 3. Notably, the thickness showed a positive relationship with the increase in components and their ratios, as illustrated in the bar graph in Fig. 3.

3.1.2 Transparency and opacity. Transparency in food-packaging films is essential for both consumer appeal and visual product monitoring during storage. Therefore, in this work, an analysis of light transmission for the prepared films was performed. Fig. 3 presents the opacity values. The least opaque (most transparent) film discovered was the C film. The amount of transparency was somewhat reduced by the addition of xanthan gum and vanillin; while the further incorporation of nanoclays, xanthan gum, vanillin, and MMT nanoclay all altered the transparency and were responsible for changes to
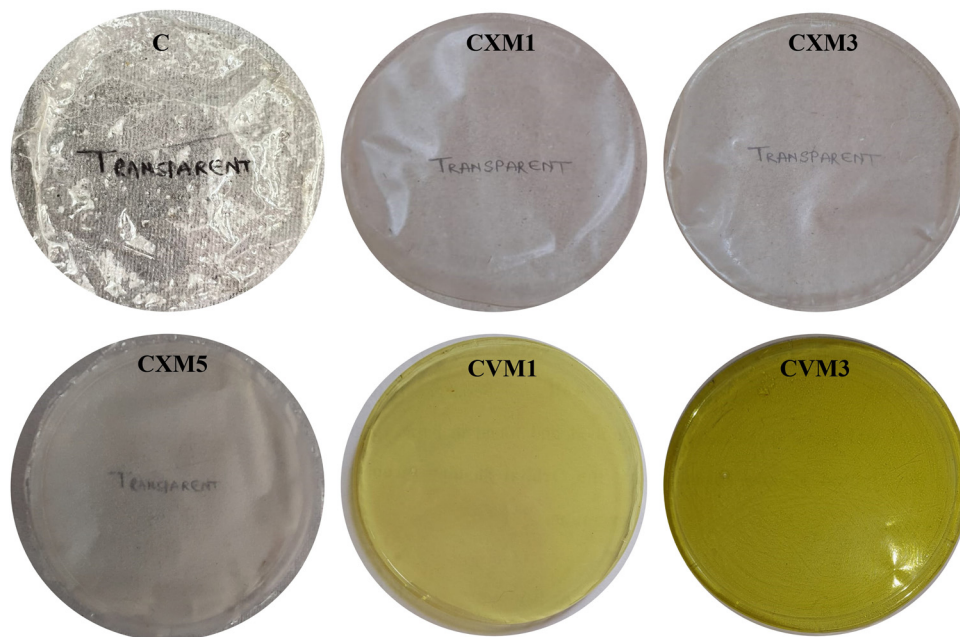
Fig. 2 Digital photos of fabricated packaging samples [pristine chitosan film (C) and chitosan and xanthan gum composites incorporated with (CXM1), 3% (CXM3) and 5% (CXM5) and chitosan–vanillin blend with reinforced MMT nanoclay 1% (CVM1), 3% (CVM3)].
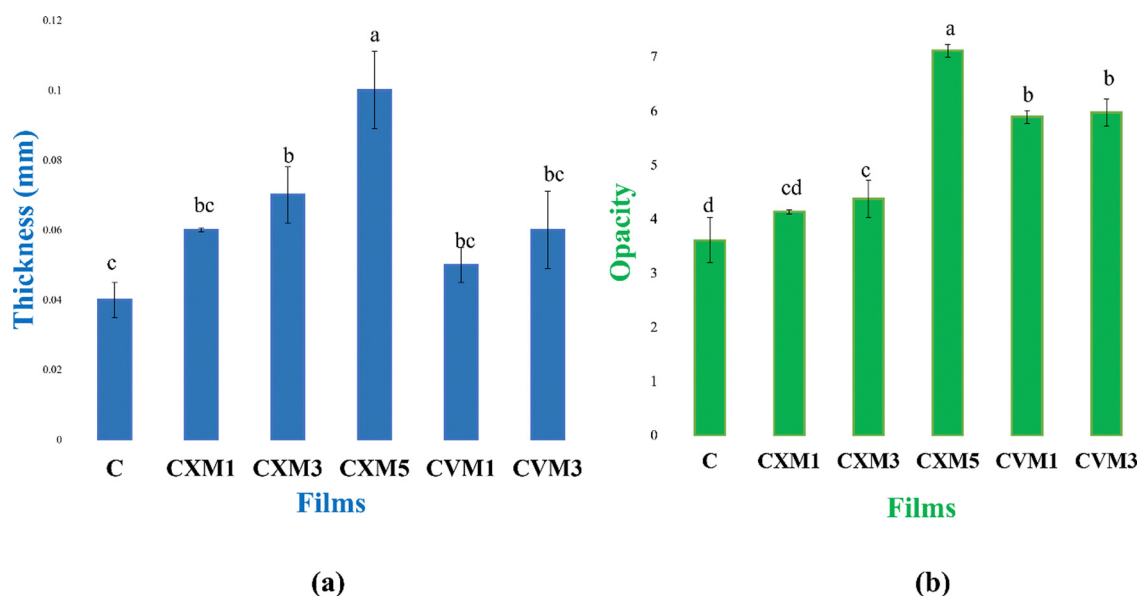

(a)

(b)

Fig. 3 (a) Thickness and (b) opacity of the synthesized films (C: pristine chitosan, CXM1: chitosan–xanthan gum composite with 1% MMT, CXM3: chitosan–xanthan gum composite with 3% MMT, CXM5: chitosan–xanthan gum composite with 5% MMT, CVM1: chitosan–vanillin composite with 1% MMT, CVM3: chitosan–vanillin composite with 1% MMT) [different letters represent significantly different values at ($p \leq 0.05$) using Tukey's test (mean ± standard deviation, n = 3)].

the color parameters. Visual scrutiny, however, indicated that all of the films were somewhat translucent. Moreover, the vanillin-based films were yellowish in color along with a nice aroma coming from the vanillin. The opacity values of the C, CXM1, CXM3, CXM5, CVM1, and CVM3 films were found to be 3.61, 4.13, 4.37, 7.11, 5.89, and 5.97, respectively, suggesting that the blends and nanofiller distributed in them were

the cause of the decrease in transparency of the chitosan film. Other scientists have reported observing something similar.[10,38,39]

3.1.3 FTIR analysis. Fourier transform infrared spectroscopy (FTIR) was employed to scrutinize the structural attributes of the films. As depicted in Fig. 4, Film C exhibited a distinctive band at 3231 cm^{-1}, indicative of the stretching
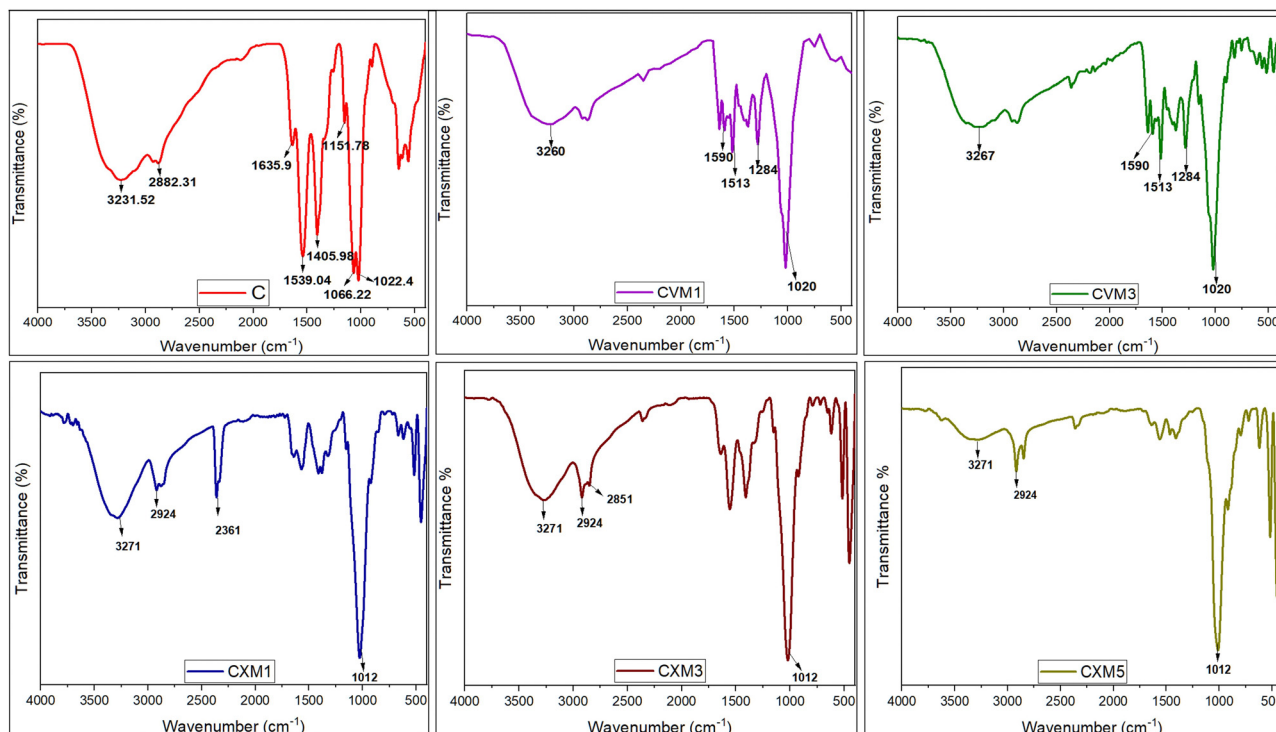
Fig. 4   FTIR spectra of all the fabricated films (C: pristine chitosan, CVM1: chitosan–vanillin composite with 1% reinforced MMT, CVM3: chitosan–vanillin composite with 3% reinforced MMT CXM1: chitosan–xanthan gum composite with 1% reinforced MMT, CXM3: chitosan–xanthan gum composite with 3% reinforced MMT, CXM5: chitosan–xanthan gum composite with 5% reinforced MMT).

vibration associated with free hydroxyl (–OH) groups, as well as symmetric and asymmetric stretching of N–H bonds within the amino groups inherent in the chitosan molecules.[28] Furthermore, the presence of a C–H bond could be discerned by the band at 2882 cm^{-1}, while the bands at 1635 and 1539 cm^{-1} were attributed to C=O stretching and N–H bending (amide I and II band), respectively.[40] Vibrational modes of symmetric deformation in the CH$_2$ group were manifested by the band at 1405 cm^{-1}, related to the vibrational modes of symmetric deformation of the CH$_2$ group,[41] while the peak at 1151 cm^{-1} was linked to the asymmetric vibrations of CO in oxygen bridges resulting from the deacetylation of chitosan.[16,42] Additional peaks at 1066 and 1022 cm^{-1} were observed, associated with the vibrational modes of –OH groups[43] in chitosan molecules. Moreover, the presence of C–O bonds was indicated by the peak at 1022 cm^{-1}.[8] All the aforementioned functional groups were anticipated constituents within the chitosan structure.[16,17]

In the 1% and 2% chitosan–xanthan gum–clay nanocomposite films, the FTIR peaks confirmed presence of strong O–H stretching and strong intermolecular H bond forming and also weak intermolecular bonding. In the 5% clay nanocomposite film, the peak of O–H stretching and strong intermolecular bonding became less intense compared to the previous two tested clay composites (1% and 3%). This indicated that the 5% clay nanocomposite film had lower and weaker intermolecular bonding. As expected from nanoclays, the addition of MMT in the chitosan framework produced a peak shift linked with NH

and OH groups, suggesting that the –NH$_2$ and –OH groups of the chitosan probably were building H-bonds with the –OH of clay.[44] The observed strong and broad peak around 3271 cm^{-1} was associated with O–H stretching and intermolecular bonds, while the peak as 2924 cm^{-1} indicated the weak intermolecular bond formation, and the additional peak at 2851 cm^{-1} corresponded to the absorption of –CH$_2$– groups.

The observed band at 3000–3500 cm^{-1} corresponded to stretching vibrations of the hydroxyl group and asymmetric and symmetric stretching of the amino (N–H) in the amino group, respectively. These were stronger in the pure chitosan film compared to in the CVM1, CVM3 films. This means that the functional group of the chitosan may be cross-linked with the vanillin.[7] There is a probability that the aldehyde group of vanillin could react with the amino groups of chitosan through physical interaction. A broad band near 1020 cm^{-1} indicated the presence of Si–O vibrations originating from the addition of montmorillonite, confirming the presence of nanoclay in the composite.[20] Finally, the peaks at 1590, 1513, and 1284 cm^{-1} were associated with vibration of the benzene ring coming from the vanillin.[18] So, analysis of the FTIR spectra indicated a clear interaction between the functional groups, namely amino and hydroxyl groups, of the chitosan molecule with xanthan gum, vanillin, and montmorillonite nanoclay.[8,16,28]

3.1.4 Mechanical parameter analysis. The mechanical properties of polymer films play a pivotal role, as they must endure typical stresses in practical applications and effectively preserve food items during distribution, transport, and storage.
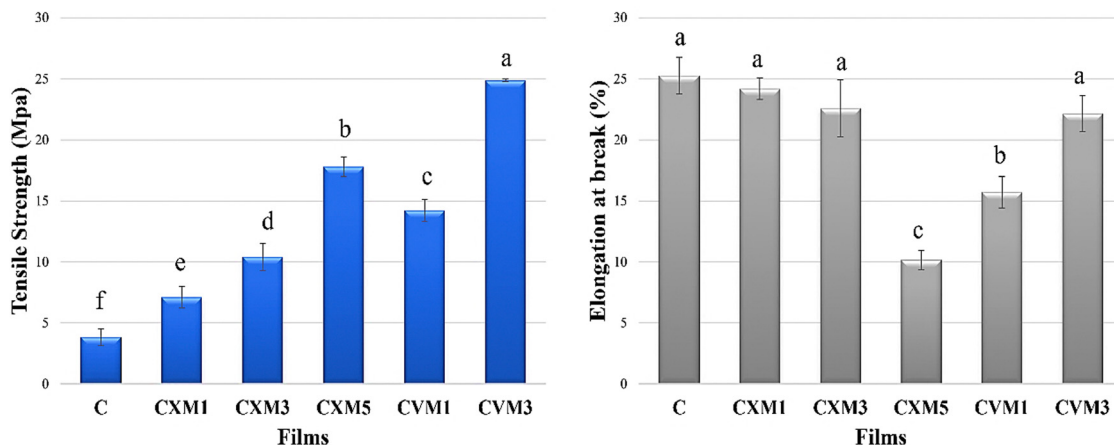
Fig. 5 Mechanical capabilities of all the manufactured films [different letters represent significantly different values at ($p \leq 0.05$) using Tukey's test (mean ± standard deviation, $n = 3$)] (C = pristine chitosan film, CXM1 = chitosan–xanthan gum blend with 1% MMT, CXM3 = chitosan–xanthan gum blend with 3% MMT, CXM5 = chitosan–xanthan gum blend with 5% MMT, CVM1 = chitosan–vanillin blend with 1% MMT, and CVM3 = chitosan–vanillin blend with 1% MMT).

Enhanced tensile properties, coupled with increased elongation, typically indicate a superior-grade material. Fig. 5 illustrates the trends for the films tested in this study, while Table 3 provides data on the strength and elongation at break for the different compositions: pristine chitosan (C), montmorillonite nanoclay reinforced chitosan–xanthan gum blends (CXM1, CXM3, CXM5), and chitosan–vanillin blends with varying weight percentages (CVM1, CVM3). The unmodified chitosan film exhibited the highest elongation percentage among all the films; however, it had the lowest strength. The results from this study reveal that, in comparison to the pure chitosan film, all the nanocomposites displayed superior tensile strengths. The incorporation of xanthan gum and montmorillonite nanoclay led to a gradual increase in tensile strength and a gradual decrease in the elongation at break. Researchers have observed that a heightened tensile strength often results from increased interactions between components, leading to improved strength and reduced flexibility.[45,46] On the other hand, the vanillin-based nanocomposite films showed a gradual increase in strength and flexibility with increasing the amount of nanoclay.[18,47,48] According to earlier reports, composite films produced with nanoclays/fibers and other nanofiller reinforcements have improved mechanical properties.[49–52] CVM3 exhibited the overall best results in terms of tensile strength and elongation at break%. Film CXM5 was the stiffest in nature, as shown as per the analysis, whereby the SEM micrographs showed a breakage of its surface, with the stiffness of the film to be blamed here.

3.1.5 Thermal analysis. Examining the thermal behavior of synthesized packaging films is crucial, given the potential impact of temperature on film stability. Thermogravimetric analysis (TGA) was employed to determine the mass change under controlled temperature conditions. This analysis provides valuable information, such as identifying the temperature range at which a sample achieves a consistent chemical composition and quantifying the rates of dehydration, oxidation, combustion, and other related events. Fig. 6 illustrates the TGA curves for each sample, conducted in a nitrogen atmosphere. In all the film thermograms, the initial thermal stage corresponded to the release of water molecules. Subsequent releases were related to the organic mass loss and thermal degradation. Notably, the pristine chitosan film retained 19.77 wt% at 500 °C at the end of the analysis. Comparatively, CVM1 and CVM3 exhibited improved thermal stability, suggesting an enhancement in film performance. CXM1, CXM3, and CXM5 also demonstrated enhanced stability compared to the control, retaining 28.00%, 31.83%, and 24.32 wt% at the end of the analysis, respectively. The ΔY value for CVM1 was 47.63% at around 280 °C, while for CVM3 the ΔY value was 50.44% at 310 °C. These values typically represent the percentage of the original mass lost during specific thermal events. The most favorable result was observed in the case of CVM3, which retained 45.74 wt% at the end of the analysis, indicating its superior thermal stability.

3.1.6 Surface morphology analysis. A comprehensive investigation of the film surfaces was conducted by field emission scanning electron microscopy (FE-SEM), and the corresponding micrographs are depicted in Fig. 7. The initial examination of the pristine chitosan film C revealed a smooth surface with minor clusters/agglomerations of undissolved chitosan particles. In contrast, the surfaces of all the bio-nanocomposites exhibited well-dispersed fillers. Notably, CXM1 and CVM1 displayed a lower presence of nanoclay on their surfaces. The incremental ratio of nanofillers was correlated with an observable increase in surface roughness for the nanocomposite films, indicative of a progressive incorporation of nanoparticles. Remarkably, the surfaces of the CXM3 and CVM3 films exhibited the most uniform distribution of nanoclay and nanoparticles, respectively, fostering greater compatibility between the filler and matrix and suggesting potential improvements in the film properties.[16] This observation aligns with the enhancements noted in other film properties. Conversely, the
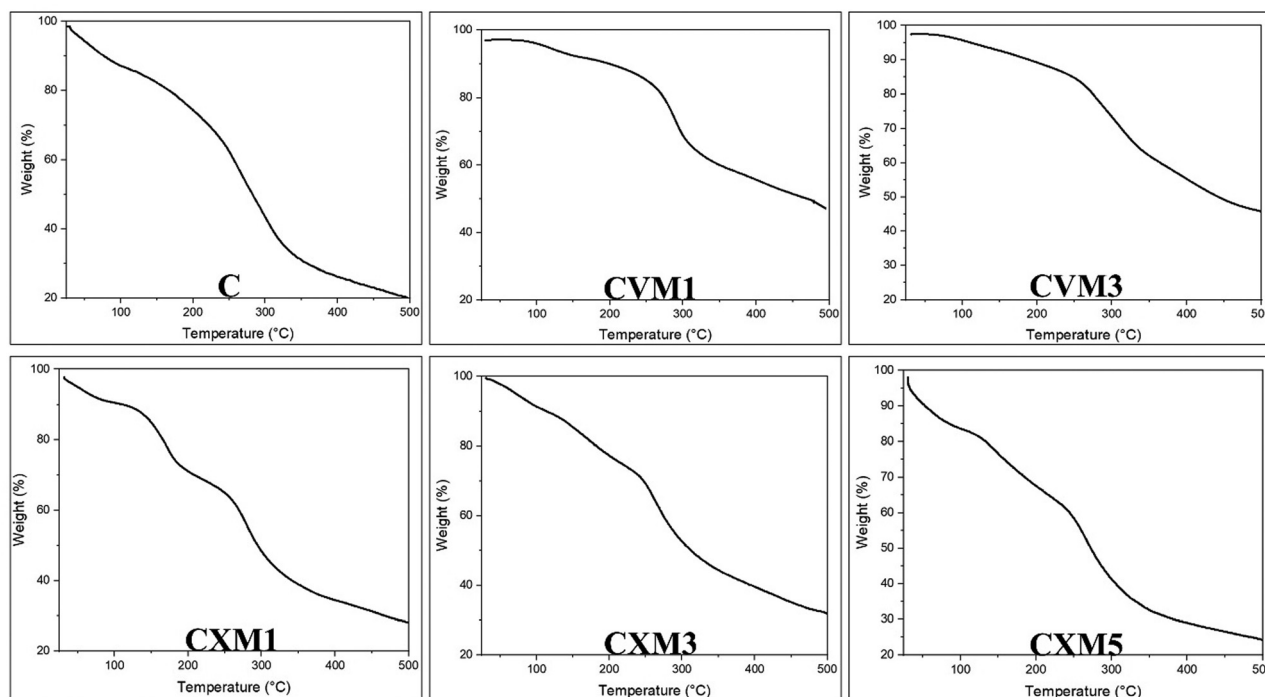
Fig. 6 Thermal analysis (C: pristine chitosan, CVM1: chitosan−vanillin composite with 1% reinforced MMT, CVM3: chitosan−vanillin composite with 3% reinforced MMT CXM1: chitosan−xanthan gum composite with 1% reinforced MMT, CXM3: chitosan−xanthan gum composite with 3% reinforced MMT, CXM5: chitosan−xanthan gum composite with 5% reinforced MMT).

surface of CXM5 revealed pore formation, likely attributed to filler aggregates, contributing to a reduced film flexibility and increased susceptibility to breakage.

3.2 Barrier ability of the fabricated packaging materials

3.2.1 Water vapor barrier. A critical determinant of the shelf life of packaged foods pertains to the film's water vapor transfer rate (WVTR), as the prompt absorption of environmental moisture can expedite product degradation and instigate microbial spoilage. Thus, an effective packaging film necessitates a robust moisture barrier. The compiled moisture transmission rates in Table 3 indicate that the parental chitosan film exhibited the highest WVTR value of 560 g m^{-2} day^{-1} due to its intrinsic hydrophilic characteristics. Notably, all the nanocomposites demonstrated enhanced moisture resistance compared to the control, attributed to the formation of a dense network through material interactions and the nanofillers' efficacy in obstructing free spaces within the matrix. CVM3 demonstrated an optimal barrier capacity with a WVTR of 245.48 g m^{-2} day^{-1}, showing a significant 56.16% improvement compared to pristine chitosan. This indicated that CVM3 was the superior formulation among all those tested, likely due to the substantial intermolecular connections within the composite.[53] In this way, a more twisted path is created within the polymeric chain, increasing its barrier properties against moisture transmission. In contrast, CXM5 displayed a comparatively higher water vapor transfer rate among the nanocomposites (Fig. 9), attributed to

the pores on the film surface (as seen in the FE-SEM micrographs in Fig. 7).

3.2.2 Gas barrier. Gas barrier testing, such as the oxygen transmission test, is crucial for evaluating the effectiveness of packaging films, as oxygen or other gases can deteriorate the quality of fresh food products. For example, oxygen exposure can lead to oxidation, spoilage, and color and texture changes that eventually affect the shelf life of produce. Fresh fruits and vegetables continue to respire even after they are harvested. The structural arrangement and vacant space in the packaging material can affect how much oxygen gas can pass through it. Consequently, the interactions of the materials and bond formations can reduce the oxygen gas permeability. According to research, the widely used LDPE food-packaging films feature a high oxygen penetration rate (OTR, 4000 cc m^{-2} day^{-1}) and weak oxygen barrier properties. High OTR values typically signify a lack of oxygen resistance across the packing film, which will fast cause microbial growth on the packaged food. All the films including the bio-based polymers and composites displayed a lower oxygen permeability than that of LDPE. However, among all the synthesized films, the pristine chitosan film possessed the highest oxygen transmission rates, whereby all the nanocomposites showed improved resistance to gas passage (Table 3). Moreover, the vanillin-based films (CVM1 and CVM3) exhibited significantly decreased oxygen transmission, in comparison to the pristine chitosan. The compressed structure formation owing to the creation of a thick network and an obstruction by the nanofillers to the pores within the
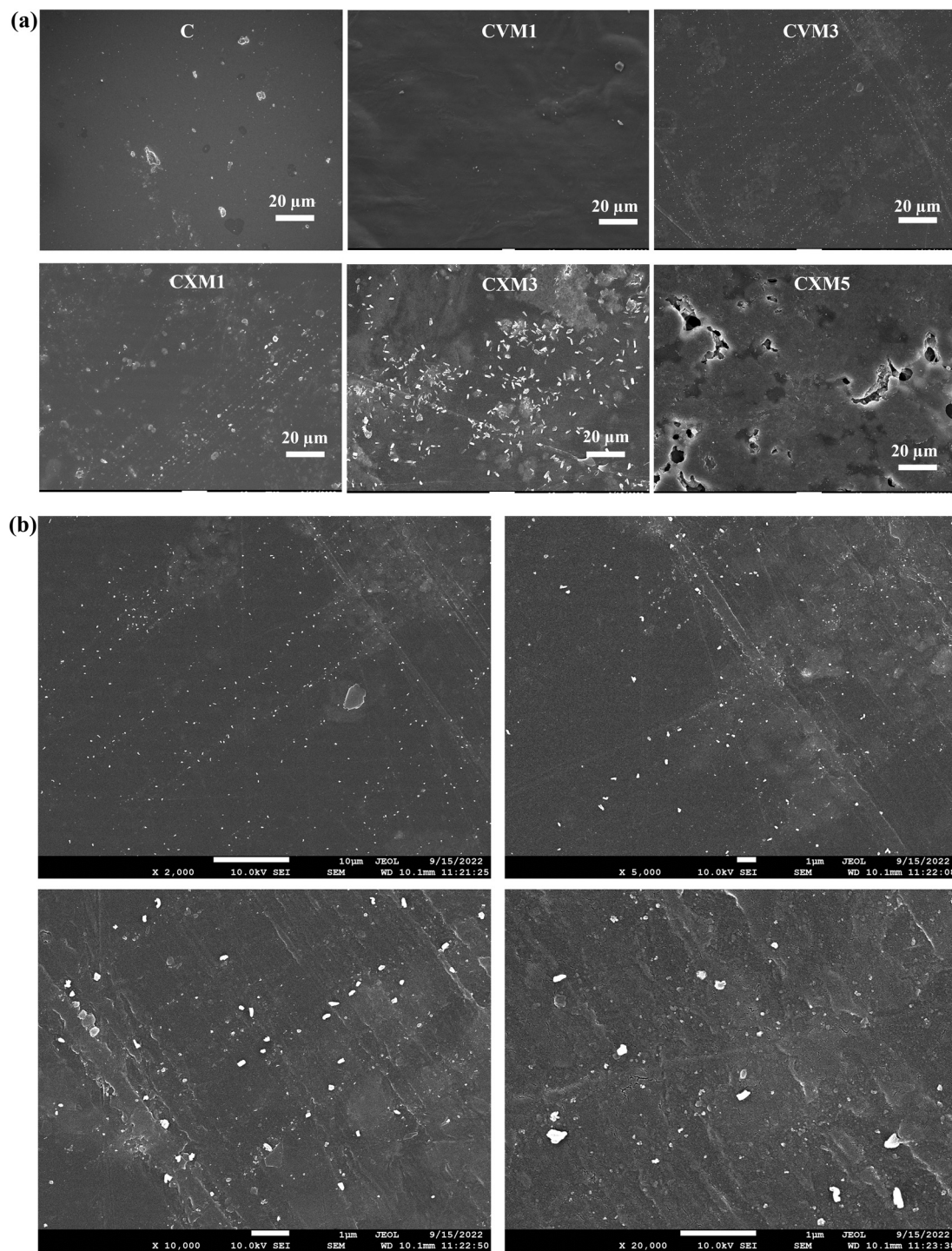
Fig. 7 (a) FE-SEM images of all the films showing their surface appearance (C: pristine chitosan, CVM1: chitosan–vanillin composite with 1% reinforced MMT, CVM3: chitosan–vanillin composite with 3% reinforced MMT, CXM1: chitosan–xanthan gum composite with 1% reinforced MMT, CXM3: chitosan–xanthan gum composite with 3% reinforced MMT, and CXM5: chitosan–xanthan gum composite with 5% reinforced MMT). (b) FE-SEM images of CVM3 (chitosan–vanillin composite with 3% reinforced MMT) at higher magnifications.

polymer matrix may be responsible for the good oxygen gas barrier results. Breakage and pore formation in the surface of the CXM5 film were possibly the reason behind the increased transmission.

3.2.3 UV barrier. To mitigate degradation, discoloration, and nutrient loss arising from exposure to UV-visible radiation, packaging materials must possess UV-absorbing capabilities. UV screening, spanning the wavelength range of 200–800 nm
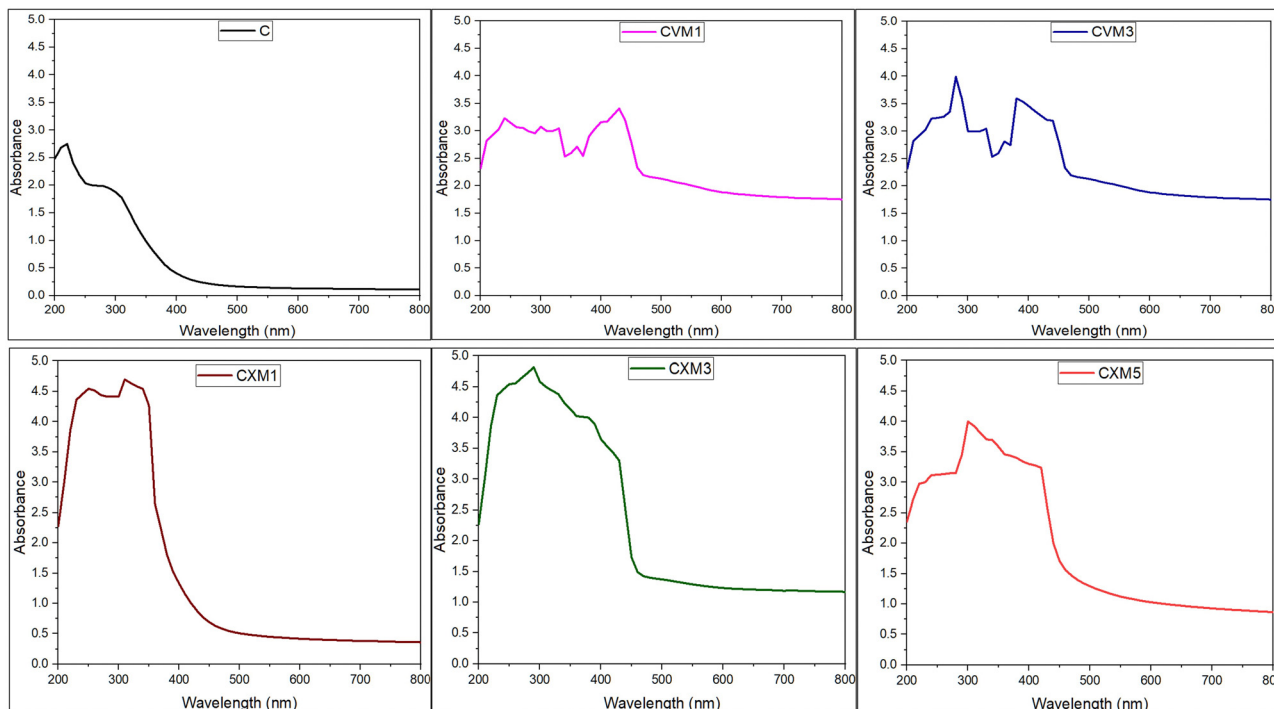
Fig. 8 UV-blocking capacity of all the manufactured films (C: pristine chitosan, CVM1: chitosan–vanillin composite with 1% reinforced MMT, CVM3: chitosan–vanillin composite with 3% reinforced MMT CXM1: chitosan–xanthan gum composite with 1% reinforced MMT, CXM3: chitosan–xanthan gum composite with 3% reinforced MMT, and CXM5: chitosan–xanthan gum composite with 5% reinforced MMT).

and conducted through spectrophotometry, revealed that the pristine chitosan exhibited the lowest absorption capacity, while the incorporation of nanofillers effectively enhanced UV-light shielding, as depicted in Fig. 8. All the bio-nanocomposites demonstrated superior absorption compared to the control, which exhibited notably low absorption in the UV range with no discernible absorption in the visible range. Notably, the nanoclay composites exhibited an

enhanced UV-blocking capacity, highlighting their superior UV-shielding properties.[54]

3.3 Water absorbency and degradability

3.3.1 Water absorbance capacity. Evaluating the water absorbency percentage of bioplastic in terms of percentage swelling is crucial when considering its practical application, as excessive water absorption can compromise a material's
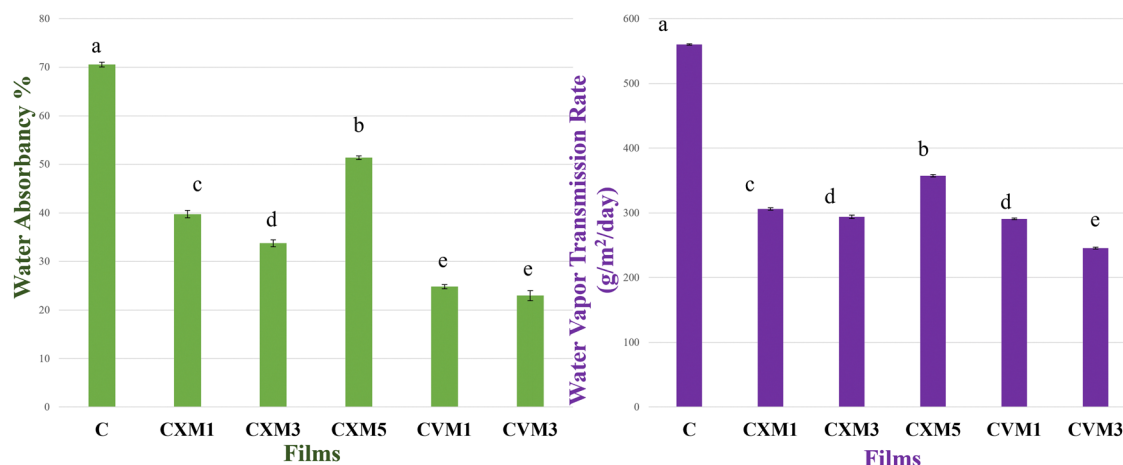

Fig. 9 Water absorbency and water vapor transmission rate of all the synthesized films [different letters within a column represent significantly different values at ($p \leq 0.05$) using Tukey's test (mean ± standard deviation, $n = 3$)].
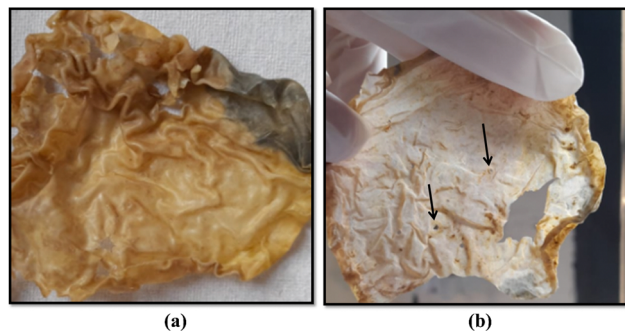
Fig. 10 Signs of biodegradation [(a) color changes and darkening of the film. (b) Formation of multiple holes in the film, a sign of bulk-erosion-type degradation].

structural integrity and functionality in various applications. The moisture absorption capacity % values of the fabricated films were evaluated and compared (Table 3). Neat film C exhibited the highest water absorbency of $70.52 \pm 1.29\%$. Compared to parental chitosan, all the nanocomposites had reduced hydrophilicity. However, among all the nanocomposites, CXM5 seemed to have the highest water absorbency, attributed to the pores in its film surface facilitating increased water uptake, as seen in the FE-SEM micrographs. Furthermore, it was observed that the chitosan–vanillin–MMT clay nanocomposite films CVM1 and CVM3 displayed optimal results, manifesting moisture absorbance decreases of 24.78 and 22.96%, respectively. The water affinity of chitosan is primarily influenced by the hydrophilic functional groups present in it, $i.e.$, hydroxyl (OH) and amino (NH_2) groups, which are mitigated by interactions with other materials in the composite, limiting their availability to engage with water molecules, subsequently reducing the nanocomposites' water absorption capacity. The absence of –OH groups in the biopolymer matrix, resulting from H-bonding with nanofillers in the various composite films, was identified as a contributory factor to the decreased moisture absorption, consistent with previous findings.[16,25,27,32,55]

(C is parental chitosan film, CXM1 is chitosan–xanthan gum blend with 1% MMT, CXM3 is chitosan–xanthan gum blend with 3% MMT, CXM5 is chitosan–xanthan gum blend with 5% MMT, CVM1 is chitosan–vanillin blend with 1% MMT, and CVM3 is chitosan–vanillin blend with 1% MMT).

3.3.2 Biodegradability. Because biodegradable films do not cause pollution, they do not endanger the environment. The type, chemical composition/modification, crystallinity, amount of the fillers employed, $etc.$ all affect the degradation process.[34] Due to their compact structure or antimicrobial properties, fillers can reduce the biodegradability of a film and increase its durability.[56–59] Polymeric materials experience considerable changes in their structure, shape, and characteristics as a result of environmental influences, such as microbes, temperature, humidity, and the pH of the medium (soil).[34] Overall, the soil burial investigations revealed a two-stage degradation process, starting with water diffusing into the film and causing it to inflate and develop microorganisms. Enzyme-based and other
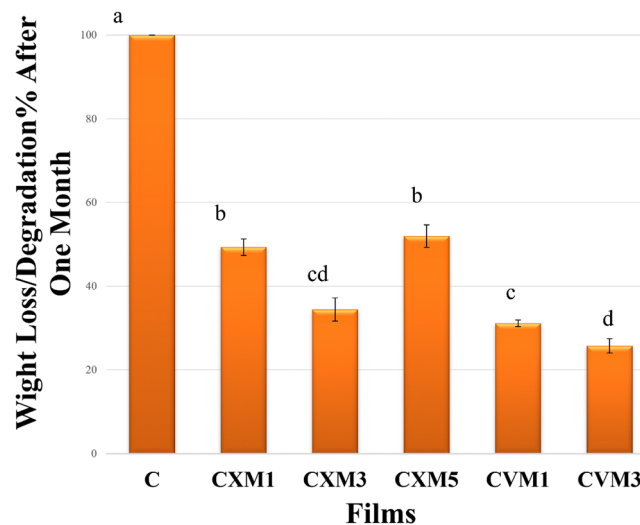

Fig. 11 Biodegradability of the films in the first month [different letters represent significantly different values at ($p \le 0.05$) using Tukey's test (mean $\pm$ standard deviation, $n = 3$)].

Table 2 Soil analysis

S. no.	Parameter	Result
1	pH	8.5 ± 0.7
2	N (nitrogen available)	633 ± 2.64 kg Ha^{-1}
3	P (phosphorus available)	266 ± 0.4 kg Ha^{-1}
4	K (potassium available)	$0.19 \pm 0.05\%$

degradation occurs in the second stage, causing a reduction in weight and film sample breakdown.[27] All the films examined for biodegradation exhibited a weight loss, structural alterations, and underwent a form of deterioration characterized as bulk erosion. Film C experienced complete degradation within the first month, while the xanthan gum–vanillin blends and the incorporation of nanoclays showed improved durability, yet maintained efficient biodegradability. Fig. 10 illustrates the evident signs of biodegradation, manifested by a color change from transparent to dark brown or black, indicative of the degradation process. The arrows in the image highlight hole formation in the film, signifying bulk erosion-type degradation. The weight loss percentages of all the biodegradable films were documented during the first month under laboratory conditions, as depicted in both Fig. 11 and Table 3. The soil samples utilized in the degradation test were subjected to physiochemical analysis. The results are depicted in Table 2 below.

4. Conclusion

Using a quick and affordable solution casting technique, MMT nanoclay was incorporated in chitosan–xanthan gum and chitosan–vanillin blended films were effectively created in the current work. To accurately characterize the films, a variety of instrumentation approaches were used. Observing all the results, it was concluded that the 3 wt% MMT-incorporated

Table 3 Properties of the synthesized films [different letters within a column represent significantly different values at ($p \leq 0.05$) using Tukey test (mean ± standard deviation, $n = 3$)]

S. no.	Film	Thickness (mm)	Opacity (%)	Tensile strength (MPa)	Elongation at break (%)	Water vapor transmission rate (WVTR) in g m⁻² day⁻¹	Water absorption capacity (%)	Degradability % (1st month)	Oxygen transmission rate (OTR) (cm³ m⁻² day⁻¹)
1	C	0.04 ± 0.005^c	3.61 ± 0.42^d	3.85 ± 0.69^f	25.27 ± 1.5^a	560 ± 1.0^a	70.52 ± 0.5^a	100 ± 00^a	1906.58 ± 1.45^a
2	CXM1	0.06 ± 0.0005^{bc}	4.13 ± 0.04^{cd}	7.1 ± 0.86^e	24.21 ± 0.88^a	306.15 ± 1.94^c	39.76 ± 0.77^c	49.27 ± 1.97^b	1783.4 ± 1.15^c
3	CXM3	0.07 ± 0.008^b	4.37 ± 0.35^c	10.41 ± 1.1^d	22.6 ± 2.34^a	293.83 ± 2.65^d	33.74 ± 0.71^d	31.12 ± 2.78^{cd}	1719.96 ± 1.5^d
4	CXM5	0.1 ± 0.02^a	7.11 ± 0.12^a	17.78 ± 0.8^b	10.15 ± 0.8^c	357.11 ± 1.94^b	51.36 ± 0.38^b	51.92 ± 2.68^b	1821.43 ± 1.6^b
5	CVM1	0.05 ± 0.05^{bc}	5.89 ± 0.12^b	14.22 ± 0.9^c	15.72 ± 1.29^b	290.86 ± 1.24^d	24.78 ± 0.42^e	34.46 ± 3.53^c	1617.83 ± 1.96^e
6	CVM3	0.06 ± 0.01^{bc}	5.97 ± 0.25^b	24.88 ± 0.12^a	22.14 ± 1.47^a	245.48 ± 1.5^e	22.96 ± 1.0^e	25.73 ± 1.72^d	1566.8 ± 1.9^f

chitosan–vanillin blend (1 : 1) exhibited the best overall results. The results from the FTIR examination showed that all the natural ingredients interacted to create high miscibility. In comparison to the pristine one, the optimized film CVM3 demonstrated a considerably improved mechanical performance (6.64 times better). When compared to pristine chitosan film, the barrier properties of the film, such as oxygen and moisture transmission rates, were decreased. The film also offered strong UV protection. Further, the calculated high levels of degradability guarantee environmental sustainability. With all of the aforementioned qualities, it is clear that this film is a viable environmentally friendly biodegradable alternative to petroleum-based synthetic plastic packaging for food.

Author contributions

Zeba Tabassum: investigation; data curation; writing – original draft; and writing – review and editing. Madhuri Girdhar: conceptualization; project administration; supervision. Tabarak Malik: resources; supervision. Anil Kumar: resources and review. Anand Mohan: conceptualization; supervision; and review and editing.

Data availability

The data supporting this article have been included as part of the ESI.†

Conflicts of interest

The authors declare no competing financial interest.

Acknowledgements

References

1 J. George, R. Kumar, B. Aaliya and K. V. Sunooj, in *BOOK*, ed. H. U. Hebbar, R. Sharma, R. S. Chaurasiya, S. Ranjan, K. Raghavarao, Springer, Cham, 2023, pp. 411–442.

2 A. Khan, S. M. Sapuan, J. Yusuf, V. U. Siddiqui, E. S. Zainudin, M. Y. M. Zuhri, B. T. H. Tuah Baharuddin, M. A. Ansari and A. A. A. Rahman, *Renewable Sustainable Energy Rev.*, 2023, **188**, 113832.

3 E. Kabir, R. Kaur, J. Lee, K.-H. Kim and E. E. Kwon, *J. Cleaner Prod.*, 2020, **258**, 120536.

4 Z. Tabassum, A. Mohan, N. Mamidi, A. Khosla, A. Kumar, P. R. Solanki, T. Malik and M. Girdhar, *IET Nanobiotechnol.*, 2023, **17**, 127–153.

5 M. Zheng, J. Chen, K. B. Tan, M. Chen and Y. Zhu, *Food Chem.*, 2022, **374**, 131794.

6 K. Kho and S. Aslanzadeh, *IOP Conf. Ser.: Mater. Sci. Eng.*, 2020, **742**, 012016.

7 Z.-H. Zhang, Z. Han, X.-A. Zeng, X.-Y. Xiong and Y.-J. Liu, *Int. J. Biol. Macromol.*, 2015, **81**, 638–643.

8 C. Rodrigues, J. M. M. de Mello, F. Dalcanton, D. L. P. Macuvele, N. Padoin, M. A. Fiori, C. Soares and H. G. Riella, *J. Polym. Environ.*, 2020, **28**, 1216–1236.

9 V. Souza, J. Pires, É. Vieira, I. Coelhoso, M. Duarte and A. Fernando, *Coatings*, 2018, **8**, 177.

10 F. Vilarinho, M. F. Vaz and A. S. Silva, *Recent Pat. Food, Nutr. Agric.*, 2020, **11**, 13–26.

11 S. İlk, M. Şener, M. Vural and S. Serçe, *J. Bionanosci.*, 2018, **8**, 1014–1020.

12 P. Cazón and M. Vázquez, in *Sustainable Agriculture Reviews*, ed. G. Crini and E. Lichtfouse, Springer, Cham, 2019, pp. 81–123.

13 A. Kramar, I. Rodríguez Ortega, G. González-Gaitano and J. González-Benito, *Cellulose*, 2023, **30**, 2037–2052.

14 S. Samal, B. Svomova, M. Spasovová, O. Tyc, D. Vokoun and I. Stachiv, *Appl. Sci.*, 2023, **13**, 1016.

15 Y. X. Xu, K. M. Kim, M. A. Hanna and D. Nag, *Ind. Crops Prod.*, 2005, **21**, 185–192.

16 Z. Tabassum, M. Girdhar, A. Kumar, T. Malik and A. Mohan, *ACS Omega*, 2023, **8**, 31318–31332.

17 M. de Morais Lima, D. Bianchini, A. Guerra Dias, E. da Rosa Zavareze, C. Prentice and A. da Silveira Moreira, *J. Appl. Polym. Sci.*, 2017, **134**(23), 44899.

18 M. Stroescu, A. Stoica-Guzun, G. Isopencu, S. I. Jinga, O. Parvulescu, T. Dobre and M. Vasilescu, *Food Hydrocolloids*, 2015, **48**, 62–71.

19 H. Palak, B. Aktürk, B. K. Kayaoğlu and İ. Göcek, *J. Ind. Text.*, 2022, **51**, 4118S–4132S.

20 C. Paluszkiewicz, E. Stodolak, M. Hasik and M. Blazewicz, *Spectrochim. Acta, Part A*, 2011, **79**, 784–788.

21 J. Sanetuntikul, K. Ketpang, P. Naknaen, B. Narupai and N. Petchwattana, *Clean. Eng. Technol.*, 2023, **17**, 100683.

22 W. Chen, S. Liang, Y. Peng, Y. Wang and T. Liu, *RSC Adv.*, 2023, **13**, 7385–7391.

23 L. Rova, H. Kurita, S. Kudo, S. Hatayama, T. Kanno, A. Gallet-Pandellé and F. Narita, *Polymers*, 2023, **15**, 1796.

24 S. Mooninta, S. Poompradub and P. Prasassarakich, *J. Polym. Environ.*, 2020, **28**, 3116–3128.

25 M. Yadav, K. Behera, Y.-H. Chang and F.-C. Chiu, *Polymers*, 2020, **12**, 202.

26 M. Yadav, Y.-K. Liu and F.-C. Chiu, *Nanomaterials*, 2019, **9**, 1523.

27 V. D. Hiremani, T. Gasti, S. P. Masti, R. B. Malabadi and R. B. Chougale, *Iran. Polym. J.*, 2022, **31**, 503–518.

28 S. K. Saral, M. P. Indumathi and G. R. Rajarajeswari, *Int. J. Biol. Macromol.*, 2019, **124**, 163–174.

29 H. Eslami and T. H. Mekonnen, *Sustainable Mater. Technol.*, 2023, **37**, e00694.

30 D. M. Seong, H. Lee, J. Kim and J. H. Chang, *Materials*, 2020, **13**, 2382.

31 M. Rezvanian, N. Ahmad, M. C. I. Mohd Amin and S.-F. Ng, *Int. J. Biol. Macromol.*, 2017, **97**, 131–140.

32 M. Yadav and F.-C. Chiu, *Carbohydr. Polym.*, 2019, **211**, 181–194.

33 H. Ismail and N. F. Zaaba, *Polym. Plast. Technol. Eng.*, 2011, **50**, 1214–1219.

34 C. Vasile, D. Pamfil, M. Râpă, R. N. Darie-Niţă, A. C. Mitelut, E. E. Popa, P. A. Popescu, M. C. Draghici and M. E. Popa, *Composites, Part B*, 2018, **142**, 251–262.

35 N. L. Tai, R. Adhikari, R. Shanks and B. Adhikari, *Int. Biodeterior. Biodegrad.*, 2019, **145**, 104793.

36 A. Homez-Jara, L. D. Daza, D. M. Aguirre, J. A. Muñoz, J. F. Solanilla and H. A. Váquiro, *Int. J. Biol. Macromol.*, 2018, **113**, 1233–1240.

37 X. Zhou, X. Liu, W. Liao, Q. Wang and W. Xia, *Carbohydr. Polym.*, 2022, **297**, 120048.

38 A. E. Giannakas and A. A. Leontiou, *Composites Materials for Food Packaging*, Wiley, 2018, pp. 1–71.

39 S. H. Othman, H. N. Ling, R. A. Talib, M. N. Naim, N. P. Risyon and Md Saifullah, *J. Nano Res.*, 2019, **59**, 77–93.

40 M. P. Indumathi, K. Saral Sarojini and G. R. Rajarajeswari, *Int. J. Biol. Macromol.*, 2019, **132**, 1112–1120.

41 S. Sanuja, A. Agalya and M. J. Umapathy, *Int. J. Biol. Macromol.*, 2015, **74**, 76–84.

42 J. C. Roy, S. Giraud, A. Ferri, R. Mossotti, J. Guan and F. Salaün, *Carbohydr. Polym.*, 2018, **198**, 281–293.

43 L.-H. Li, J.-C. Deng, H.-R. Deng, Z.-L. Liu and L. Xin, *Carbohydr. Res.*, 2010, **345**, 994–998.

44 X. Wang, Y. Du, J. Yang, X. Wang, X. Shi and Y. Hu, *Polymer*, 2006, **47**, 6738–6744.

45 S. W. Lee, N. S. Said and N. M. Sarbon, *J. Food Sci. Technol.*, 2021, **58**, 4294–4302.

46 E. Butnaru, E. Stoleru, M. Brebu, R. Darie-Nita, A. Bargan and C. Vasile, *Materials*, 2019, **12**, 373.

47 S. S. Narasagoudr, V. G. Hegde, V. N. Vanjeri, R. B. Chougale and S. P. Masti, *Carbohydr. Polym.*, 2020, **236**, 116049.

48 B. Tomadoni, A. Ponce, M. Pereda and M. R. Ansorena, *Polym. Test.*, 2019, **78**, 105935.

49 V. Dharini, S. Periyar Selvam, J. Jayaramudu and R. Sadiku Emmanuel, *Appl. Clay Sci.*, 2022, **226**, 106555.

50 N. Bumbudsanpharoke and S. Ko, *J. Nanomater.*, 2019, **2019**, 1–13.

51 W. Wu, Y. Wu, Y. Lin and P. Shao, *Food Chem.*, 2022, **374**, 131763.

52 M. L. C. de Oliveira, S. Mirmehdi, M. V. Scatolino, M. G. Júnior, A. R. Sanadi, R. A. P. Damasio and G. H. D. Tonoli, *Cellulose*, 2022, **29**, 1097–1113.

53 G. Lavrič, A. Oberlintner, I. Filipova, U. Novak, B. Likozar and U. Vrabič-Brodnjak, *Polymers*, 2021, **13**, 2523.

54 H. Moustafa, S. M. El-Sayed and A. M. Youssef, *J. Thermoplast. Compos. Mater.*, 2023, **36**, 96–117.

55 S. Mitura, A. Sionkowska and A. Jaiswal, *J. Mater. Sci.: Mater. Med.*, 2020, **31**, 50.

56 T. Glaskova-Kuzmina, O. Starkova, S. Gaidukovs, O. Platnieks and G. Gaidukova, *Polymers*, 2021, **13**, 3375.

57 N. Neibolts, O. Platnieks, S. Gaidukovs, A. Barkane, V. K. Thakur, I. Filipova, G. Mihai, Z. Zelca, K. Yamaguchi and M. Enachescu, *Mater. Today Chem.*, 2020, **17**, 100301.

58 O. Platnieks, S. Gaidukovs, V. Kumar Thakur, A. Barkane and S. Beluns, *Eur. Polym. J.*, 2021, **161**, 110855.

59 Z. Tabassum, A. Mohan and M. Girdhar, *AIP Conf. Proc.*, 2024, **2986**, 030044.